2016–2017

MASTER DE CHIMIE DE PARIS CENTRE

Spécialité : Chimie Analytique, Physique et Théorique

Internship Report 5C101

Managing triplet excitons in singlet fission sensitised pentacene solar cells

Lucie Mc Govern

Under the supervision of Bruno Erhler

Amolf Institute, the Netherlands

Contents

1 Introduction

1.1 Organic semiconductors

Organic semiconductors are a class of materials that combine the electronic advantages of semiconducting materials with the chemical and mechanical benefits of organic compounds such as plastics. Thus, the ability to absorb light, conduct electricity, and emit light is united with a material structure that can be easily modified by chemical synthesis, for example, to tailor electronic properties such as the desired emission wavelength or to allow for mechanically robust, light-weight and flexible thin films.

Solar cells are devices that allow the conversion of light to electrical current. Specifically, organic solar cells have been developed since the late 1980s when the first demonstration of a dye sensitized solar cell was made[1]. The research nowadays aims to develop new materials, both highly-efficient and cheap. In this context, multiple exciton generation processes observed in organic semiconductors are promising.

1.2 Singlet fission

Singlet fission is an efficient multiple exciton generation process in organic semiconductors, by which a high-energy singlet exciton is converted into two triplet excitons of lower energy,which can be seen in Figure 1 in terms of an energy level diagram. The green arrow represents the absorption of a photon leading to the generation of an excited singlet exciton labeled S_1 and the purple arrow represents the singlet fission process itself: the excited singlet exciton S_1 is converted to two triplet excitons T_1. While the mechanism of singlet fission is the subject of intense study[2]-[4], it is generally agreed that the photoexcitation generates a triplet pair $^1(TT)$ state either coherently or uncoherently from the singlet exciton, and that this state may subsequently separate into two triplets $(2 \times T_1)$ in an overall spin-allowed process[5].

There is an energy requirement for singlet fission to occur with a high yield: the energy of the singlet state needs to be higher or equal to the energy of the two triplets, i.e. $E(S_1) \geqslant 2E(T_1)$. This helps rationalise for the small amount of organic molecules that exhibit singlet fission.

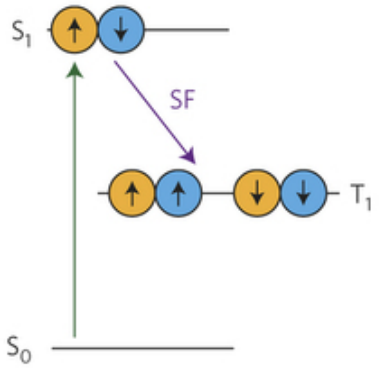

Figure 1: Schematic of singlet fission, adapted from [6]. The green arrow indicates the excitation of a molecule from its ground state S_0 to the excited state S_1. The excited state can then undergo singlet fission by exciting a neighbouring molecule to generate two triplet states T_1.

1.3 Singlet fission sensitised solar cells

Shockley and Queisser derived a theoretical limit of 34% for the efficiency of a conventional single-junction solar cell illuminated by the sun[8]. There are two main factors limiting the power conversion efficiency of such cells. The first limit arises because photons with an energy below the bandgap of the semiconductor are not absorbed. The second limit is due to photons with an energy higher than the bandgap as they loose this excessive energy as heat, in the so-called thermalisation loss.

Singlet fission is a promising way of overcoming the thermalisation losses. As mentioned previously, a high-energy photon generates a high-energy singlet exciton which is in turn converted to a pair of triplet excitons. If these triplet excitons are successfully dissociated at the interface with an appropriate electron acceptor, the energy of both triplet excitons can be harvested and used for power generation. To convert twice as much energy from high-energy photons compared to conventional designs, i.e. to overcome the theoretical Shockley-Queisser limit, we need the combination of a singlet fission layer with an acceptor material that is also capable of harvesting low energy photons. In this configuration, the low-bandgap semiconductor generates one electron–hole pair for each low-energy photon absorbed, and simultaneously the singlet exciton fission material generates two triplet excitons for each high-energy photon absorbed. There are a limited number of possible ways to obtain such a configuration, the first is a tandem cell, the second is a device with a singlet fission layer on top of a low-bandgap inorganic semiconductor layer with either charge transfer or energy transfer between both layers. This theoretically allows a power conversion efficiency of up to 44%[9]: in figure 2 we compare the areas of the solar spectrum that are harvested in the case of a single-junction solar cell and with an added singlet fission layer.

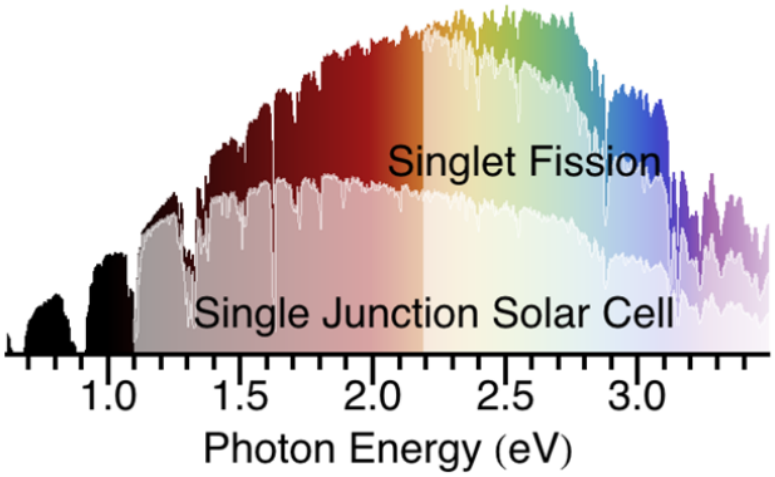

Figure 2: Representation of the solar spectrum and the added benefit of a singlet fission layer compared to a single junction solar cell used on its own, adapted from [7]. The y axis represents the solar irradiance in arbitrary units.

An additional energy requirement appears when moving from a single material layer exhibiting singlet fission to an integrated singlet fission based solar cell which comprises the electron donor - the singlet fission material itself- and the electron acceptor. Indeed, the energy of the charge-transfer state -as estimated from the difference between the HOMO of the electron donor and the LUMO of the electron acceptor- should be lower than the energy of the singlet fission generated triplet excitons, i.e. $E(T_1) > E(CT)$. This allows the exciton dissociation process at the interface to be thermodynamically favourable.

To obtain highly efficient devices, one must first understand the dynamics within the singlet fission layer, specifically the triplet exciton diffusion length. The radiative decay of triplet excitons is spin-forbidden, so for long triplet exciton diffusion lengths it is key to understand the non-radiative decay processes in detail. So far these non-radiative decay processes have been largely unexplored. In this study, we aim to investigate one of the main non-radiative decay process, charge trapping. To do so, we will study trap states and their influence on triplet exciton diffusion lengths and device performance.

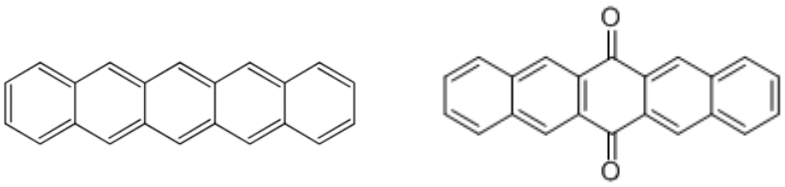

Figure 3: Pentacene molecule (left) and one of the byproducts of its oxydation, the pentacenequinone molecule (right).

Pentacene is a model system to study singlet fission, as transient absorption studies have shown that singlet fission in pentacene occurs on a timescale of 80 fs[10], thus outcompeting decay mechanisms of singlet excitons and providing for an exceptional yield of 200% triplet excitons. This feature, combined with pentacene's high absorption and good hole mobility, make pentacene the ideal candidate to study the effects of traps in singlet fission sensitised solar cells. The structure of the pentacene molecule and the structure of the pentacenequinone molecule, a trap identified as a key chemical defect in pentacene matrices are shown in Figure 3. Pentacenequinone is a byproduct of the oxydation of pentacene and has be shown to act as a deep trap for electrons[11], as well as lowering carrier mobility[12] and influencing the hole barrier injection between pentacene and electrodes[11].

2 Methods

Triplet exciton diffusion length is challenging to study as the triplet excitons are non-luminescent. This means we must find an indirect way of estimating the diffusion length of the pentacene excitons in the solar cell devices. Our method is described in the next paragraph.

We fabricate singlet fission solar cells with varying pentacene thicknesses and use a numerical model which takes into account the generation, diffusion and decay of the excitons by the active layers of the solar cell device. We then measure the experimental External Quantum Efficiency (EQE) curves of the different devices and use our model to find the best fit for the corresponding diffusion length. To investigate the effect of trap states, we compare solar cells with a pure pentacene layer with solar cells where we have added impurities to the pentacene layer.

2.1 Solar cell fabrication

We reproduce with slight modifications a device architecture first reported by M. Tabachnyk [13]. The arrangement of the device is "sandwich-type" i.e. the organic semiconductor layers are sandwiched between the electrodes, and current flows perpendicular to the semiconductor film. The active donor and acceptor layers are not mixed -as in the case of a bulk heterojunction device- but are spatially separated, thus forming a planar heterojunction device.

The device itself consists of 5 different layers: PEDOT:PSS, P3HT, pentacene, C_{60} and BCP in between two electrode layers of ITO and silver. A scheme of this device and a top picture of it are shown in Figure 4. Pentacene and C_{60} are the two main active layers of the device, both can generate excitons which are dissociated at the interface to form electrons and holes which are then transported

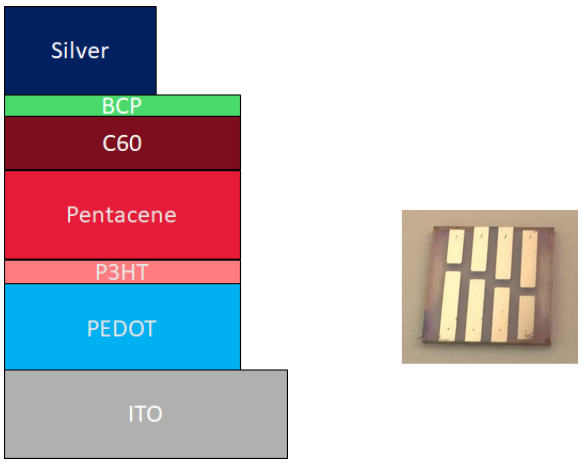

Figure 4: Architecture of the planar heterojunction device and top picture of one of the such fabricated solar cells. The 8 pixels are clearly visible in the picture.

respectively to the silver electrode and the ITO electrode. P3HT can also be counted as an active layer of the device: as shown in previous reports[13], this layer acts both as an exciton donating layer for pentacene and as a triplet exciton blocking layer for triplet excitons formed in pentacene. BCP is not an active layer in the device, but serves to block excitons at the back interface of C_{60}. We modify the design found in M. Tabachnyk's work [13] by adding a layer of PEDOT:PSS. The idea is to limit the losses at the ITO/P3HT interface. Our results do not allow to confirm this hypothesis but we notice experimentally that the stability of the solar cells -by which we mean the protection against short circuits- is enhanced.

We come back briefly on our choice of C_{60} as the acceptor material. Ehrler *et al* reported pentacene-based cells using nanocrystals as the acceptor[14]. The bandgap of nanocrystals can be tuned with their size to optimise the efficiency[15]. However, the pentacene contribution in this cell has been too low to provide direct evidence for fission. This is why we choose an alternative for the acceptor, the fullerene C_{60}. Although its bandgap is too high to form a fission-enhanced device, it facilitates the investigation of pentacene due to its good charge separation and transport properties as well as controllable processing[16].

A common choice for the back contact electrode is Indium Tin Oxide (ITO) because it combines good transparency with high conductivity. Silver is used for its very good conductivity and its low transparency which allows for some reflection of light back into the device. For tandem solar cells, a cathode combining good conductivity and good transparency is needed.

We fabricate a collection of devices by fixing the thickness of the ITO, PEDOT:PSS, BCP and silver layers -respectively 150 nm, 38 nm, 10 nm and 100 nm- and playing both with the thicknesses of the pentacene and the C_{60} layers, and with the nature of the pentacene layer, either pure pentacene or pentacene coevaporated with 20% pentacenequinone. Each device was made twice to ensure reproducibility of our results.

2.2 External quantum efficiency model

The model used to calculate the EQE of the solar cells consists of three distinct steps: the optical modeling of the multi-layer system to obtain the exciton generation profile; the resolution of the diffusion equation to obtain the local exciton density profile; and the calculation of the photocurrent density and EQE derived by the excitons dissociating at the interface. For the first step, we use the code[17] written by G. Burkhards and his coworkers, while the second and third steps were performed following work from M. Tabachnyk *et al*[13].

2.2.1 Basics of solar cell operation

In order to do model the EQE, we have to understand the operation of a solar cell based on pentacene and C_{60}. Figure 5 shows the physical processes at play in the pentacene layer from the absorption of a photon to the charge separation at the interface with C_{60}.

The first thing to mention from Figure 5 is that the pentacene-C_{60} system does indeed respect the two energy requirements mentioned in the introduction for an efficient fission sensitised solar cell : $E(S_1) > 2E(T_1)$ and $T_1 > CT$.

We can divide the processes taking place in the pentacene layer within three categories :

- the generation of excitons, in this case we consider both the absorption of a photon generating a singlet exciton and the very rapid singlet fission that follows to form two triplet excitons, represented by steps 1 and 2 in Figure 5;
- the diffusion of excitons through the layer, from their generation site to the interface with C_{60}, represented by step 3 in Figure 5;
- the non-radiative decay of excitons within the layer, which is not represented in Figure 5.

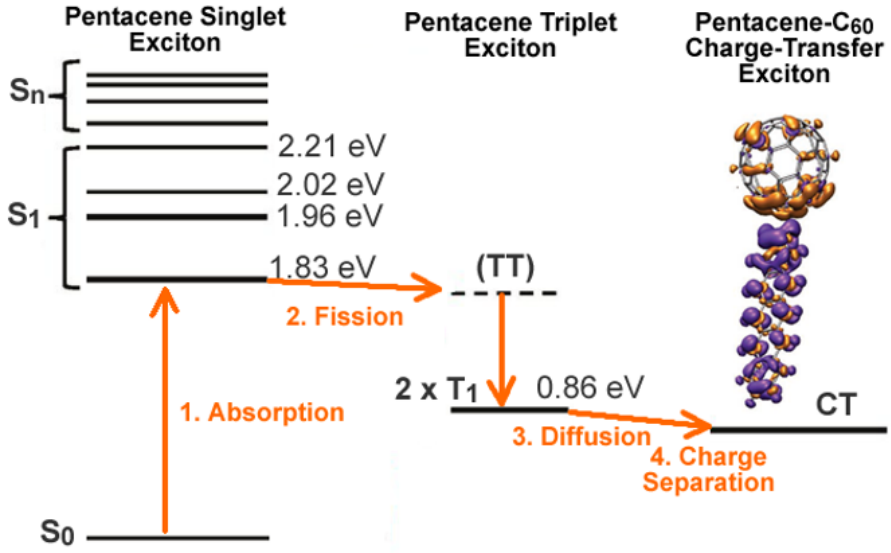

Figure 5: Energy diagram with steps of solar cell operation, adapted from [18]. The first step is the absorption of a photon, exciting a pentacene molecule from its ground state S_0 to its excited state S_1 of energy 1.83 eV. The excited state can then undergo singlet fission to generate two triplet states T_1 of energy 0.86 eV. The third step is the diffusion of the triplet excitons within the pentacene material. The fourth and final step is reached at the interface between the pentacene and the organic acceptor molecule C_{60}, where the exciton is dissociated to form two charges.

The diffusion of triplet excitons, step 3 in Figure 5, is mediated by Dexter energy transfer[19]. The actual exchange of electrons between donor and acceptor may happen when they are only about 1 nm apart, so there is significant overlap of molecular orbitals[20]. In the continuous limit the interlayer hopping can be described as 1D diffusion perpendicular to the layers. This will be an important basis for the development of our diffusion equation.

2.2.2 Exciton generation profile

The generation profile is the position-dependent probability density for the absorption of a single incident photon. It is calculated using the transfer matrix formalism for multilayer systems. In the code demonstrated by Bukhard and coworkers[17], we can adjust for the different materials and their relative thicknesses to obtain the generation profile of each layer.

Figure 6 shows the fraction of light absorbed by each layer of a device composed of 8 nm of P3HT, 20 nm of pentacene and 30 nm of C_{60}. In order to increase the short-circuit current J_{SC}, harvesting a large portion of the solar spectrum is important, which -in the case of organic semiconductors- is particularly challenging for the red and near-infrared spectral regions. To meet this requirement, the

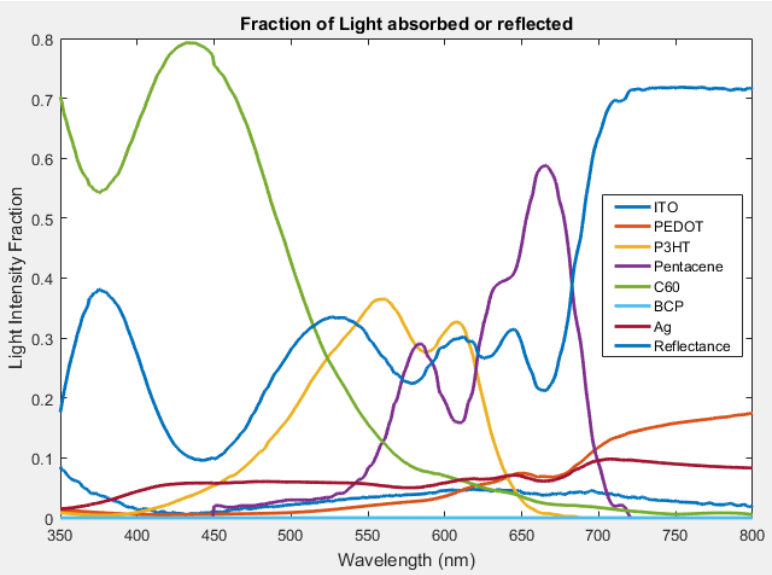

Figure 6: Fraction of light absorbed by each layer of the device and reflection of the total device, for a structure composed of 8 nm of P3HT, 20 nm of pentacene and 30 nm of C_{60}.

absorption spectra of donor and acceptor materials should preferably complement one another, as is the case in the pentacene/C_{60} combination. Indeed, C_{60} absorbs mostly in the region from 400 nm to 500 nm, and pentacene absorbs in the region from 550 nm to 700.

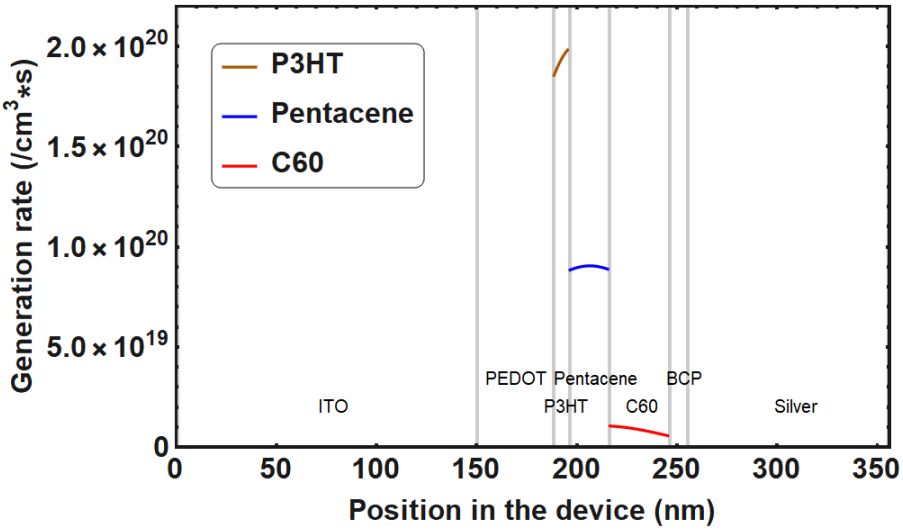

Figure 7: Generation of excitons as a function of the position in the device, at $\lambda = 600$ nm, for a structure composed of 8 nm of P3HT, 20 nm of pentacene and 30 nm of C_{60}.

Figure 7 shows the generation profile at $\lambda = 600$ nm for the active layers of a device composed of 8 nm of P3HT, 20 nm of pentacene and 30 nm of C_{60}. The absorption coefficient of both P3HT and pentacene are high at $\lambda = 600$ nm. This results in the generation profile seen in Figure 7, where most of the photons are absorbed in the first layer (i.e. a high generation profile), a small fraction is

absorbed by the second layer and only a very small fraction is absorbed by the third layer (i.e. a low generation profile).

2.2.3 Local exciton density calculation

This step -which is numerically the longest- involves the calculation of the local exciton density $n(x)$ in the 2 active layers of the device, pentacene and C_{60}. We have focused so far on the pentacene layer but the processes described in the previous section -diffusion, decay and generation of excitons- have to be considered in both active layers. Incorporating diffusion (first term), monomolecular recombination (second term) and generation (third term), we obtain the following differential equation for the local exciton density $n(x)$ in equilibrium :

$$D\frac{d^2n(x)}{dx^2} - \frac{D}{L^2}n(x) + G(x,\lambda) = 0$$

with D the diffusion constant of the exciton in the material, L the diffusion length of the exciton and $G(x,\lambda)$ the exciton generation profile as a function of position in the device and wavelength. For each wavelength λ, we resolve this equation twice, the first time for pentacene, the second for C_{60}. We do not perform diffusion modelling in P3HT since the layer is only 8 nm thin and on the order of electron delocalisation[21].

To resolve the differential equation numerically, additional boundary conditions have to be introduced in the model. These boundary conditions have a physical meaning as they describe the nature of the 2 interfaces -front and back- of each active layer.

The first boundary lays between the P3HT layer and the pentacene layer, this is the front interface for pentacene. P3HT acts as an antenna material, which means this material extends the photocurrent generated by singlet fission by donating excitons into pentacene. We thus describe the interface as an an injecting boundary:

$$Dn(x_0) = 2\eta_{P3HT}G_{P3HT}$$

with G_{P3HT} the exciton generation rate in P3HT, $G_{P3HT} = \int_{x_0}^{x_{max}} G_{P3HT}(x)$ and η_{P3HT} the injection efficiency of P3HT excitons into pentacene.

The second boundary lays between the pentacene and the C60 layers, it is both the back interface for pentacene and the front interface for C_{60}. It is the main exciton extracting boundary:

$$n(x_I) = 0$$

The third boundary is between C_{60} and BCP, it is the back interface for C_{60}. BCP is used as an exciton blocking layer, the interface can thus be described as an exciton reflecting boundary :

$$n'(x) = 0$$

This calculation is repeated in a loop that runs from $\lambda = 450$ nm to $\lambda = 800$ nm each 5 nm. Figure 8 shows the resolved local exciton density $n(x)$ at a given wavelength of $\lambda = 600$ nm, for a structure composed of 8 nm of P3HT, 20 nm of pentacene and 30 nm of C_{60}.

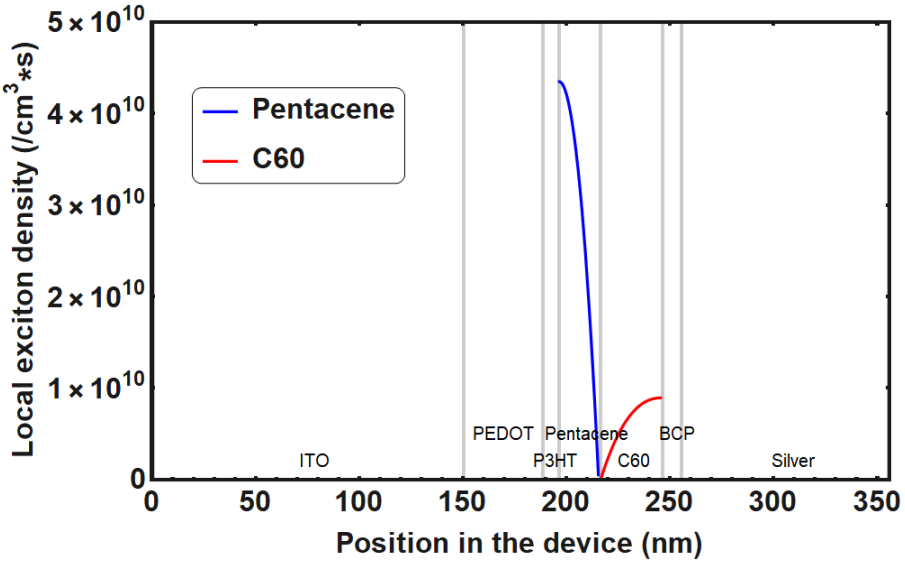

Figure 8: Local exciton density $n(x)$ as a function of the position in the device, at $\lambda = 600$ nm.

The local exciton density profile $n(x)$ respects the imposed extracting boundary condition at the pentacene/C60 interface: there are virtually no excitons at the interface. The high bending that this condition imposes on $n(x)$ close to this interface will be reflected in the calculation of a high EQE value for both materials at $\lambda = 600$ nm. This will be further explained in the following section.

2.2.4 Photocurrent and external quantum efficiency calculation

The next step of our model consists in using the local exciton density function we have calculated to extract the photocurrent derived by each active layer. For dissociation the exciton needs to reach an interface with an electron or hole acceptor material.

For the pentacene layer, as mentioned previously, C_{60} serves as the electron acceptor material, and the photocurrent derived by this active layer is written:

$$J_{pent} = \eta_{pent} eD \frac{dn_{pent}(x)}{dx}|_{x=x_I}$$

where I is the interface between pentacene and C_{60}, and η_{pent} is the efficiency of the pentacene exciton dissociation at this interface. The equation is similar for the C_{60} layer, where pentacene plays the role of the hole acceptor material:

$$J_{C60} = \eta_{C60} eD \frac{dn_{C_{60}}(x)}{dx}|_{x=x_I}$$

where I is also the interface between pentacene and C_{60}, and $\eta_{C_{60}}$ is the efficiency of the C60 exciton dissociation at this interface. A high bending of the local exciton density $n(x)$ at the interface is reflected in high values of $\frac{dn(x)}{dx}|_{x=x_I}$, which will thus lead to high values of photocurrent J, according to the two previous equations. To resolve the diffusion equation for C_{60}, we need the diffusion length of excitons in C_{60}: the value $L_{C_{60}} = 40$ nm is taken from literature[22].

Since there is no direct dissociation of excitons into charges between the P3HT layer and the pentacene layer, only excitons that have been injected from P3HT into pentacene and further dissociated at the pentacene/C_{60} interface will contribute to the photocurrent. The equation for the photocurrent derived by this layer is thus written differently:

$$J_{P3HT} = 2\eta_{P3HT}\eta_{pent} eDG_{P3HT}$$

with G_{P3HT} the exciton generation rate in P3HT, and η_{P3HT} the injection efficiency of P3HT excitons into pentacene.

The final step is to use the calculated photocurrent to find the corresponding EQE value. We do this numerically using:

$$EQE = \frac{electrons/sec}{photons/sec} = \frac{J(\lambda)/e}{\mathrm{AM1.5G}(\lambda) \times \lambda / h.c}$$

where AMG1.5 is the standard terrestrial solar spectral irradiance distribution for an air mass of 1.5. The value 1.5 represents the effective atmosphere thickness crossed by the solar light before reaching the Earth at mid-latitudes.

The EQE of P3HT, pentacene and C_{60} are calculated for each wavelength within the loop mentioned previously, i.e. every 5 nm between $\lambda = 450$ nm and $\lambda = 800$ nm. The total EQE is simply the sum of each contribution: $\mathrm{EQE_{total}} = \mathrm{EQE_{P3HT}} + \mathrm{EQE_{pent}} + \mathrm{EQE_{C_{60}}}$. There are four fitting parameters in our model, the two efficiencies for the dissociation of excitons, η_{pent} and $\eta_{C_{60}}$, the efficiency for the injection of excitons η_{P3HT} and the exciton diffusion length in pentacene L_{pent}. We will calculate different EQE curves with varying combinations of the fitting parameters, and aim to find a global set of fitting parameters that reproduce the experimental EQE curves. This method would thus allow us to estimate L_{pent}.

3 Experimental

The next section presents the experimental techniques used for this study.

3.1 Solar cell fabrication

Substrate cleaning To fabricate the solar cells, glass substrates covered with a 150 nm thick ITO stripe were cleaned in 4 successive ultrasonic baths of 15 minutes each: water and soap, water, acetone and isopropanol. The substrates were further cleaned by an oxygen plasma treatment for 30 minutes. All fabrication steps except the cleaning and the spin coating of PEDOT:PSS were done in a nitrogen environment with oxygen levels below 10 ppm and water levels below 1 ppm to avoid material degradation.

Spin coating of PEDOT:PSS and P3HT PEDOT:PSS solution was filtered using a 0.45μm GHP membrane. 80μL of the solution were spin coated onto the substrates at 4000 rpm for 60 seconds. P3HT was dissolved in chlorobenzene at a concentration of 4 mg/mL and heated at 60°C for at least 2 hours. The solution was then filtered using a 0.2μm PTFE membrane. 70μL of the solution were spin coated onto the substrates at 2000 rpm for 60 seconds to obtain thin films.

Evaporation of organic molecules and silver top contact All layers of pentacene, C_{60}, BCP and silver were sublimed in vacuum with pressures below 2×10^{-6} mbar. The evaporation rate was measured with a quartz crystal microbalance in the deposition beam and stabilised to a value dependent on the material: $1 \pm 0.2 A/s$ for pentacene, $0.5 \pm 0.1 A/s$ for C_{60} and BCP. The silver was thermally evaporated at $0.5 \pm 0.1 A/s$ for the first 10 nm and then at $1 \pm 0.2 A/s$ for the remaining 90 nm. Pentacene layer thicknesses of 20, 30, 40, 60 and 80 nm were fabricated. Different thicknesses for the C60 layer were tested: 25 nm, 30 nm and 35 nm. Prior to silver coating, the vacuum was broken in order to add a mask between the sample holder and the cells. This mask allows us to obtain 8 different pixels with each cell: two of 1.35 mm^2, two of 2.75 mm^2, two of 4.15 mm^2 and two of 5.55 mm^2.

3.2 Atomic Force Microscopy

Measurements with an atomic force microscope (AFM) were used both to analyse the surface morphology of the spin coated and thermally evaporated films, and to determine the thickness of the layer by scratching the films with a sharp needle and measuring the step height in an AFM scan. The measurements were made with a Bruker Dimension Icon system using tapping mode AFM with a ScanAsyst-air probe.

3.3 Current-Voltage measurements

The photocurrent was measured at different voltages using a Keithley 2636A source measure unit while illuminated by an Oriel 92250A solar simulator. The solar simulator produces approximately the natural sun spectrum and its intensity was calibrated with a silicon reference photodiode to $100\frac{\text{mW}}{\text{cm}^2}$. Each solar cell is divided in 8 different pixels, which are measured one after the other. The best pixel is the one we choose to measure EQE.

3.4 External quantum efficiency measurements

We use an Oriel instruments QuantX-300 to measure all EQEs. Before measuring the devices, a calibration silicon solar cell was measured.

4 Results and Discussion

4.1 Film quality

This section focuses on the results provided by the AFM data on the layers of our solar cells. As mentioned in the experimental section, we use AFM for two main purposes: the first is to determine the roughness and surface morphology of each layer of the device, the second is to determine the effective thickness of each layer. The 5 samples that we measure are prepared in the following manner: a layer of PEDOT:PSS only, a layer of PEDOT:PSS and a layer of P3HT, etc until the last sample consists of the 5 layers of PEDOT:PSS, P3HT, pentacene, C_{60} and BCP on top of each other. For page constraints reasons, we show here the results for the device containing the 3 first layers, with pentacene on top, and for the device containing the 4 first layers, with C_{60} on top.

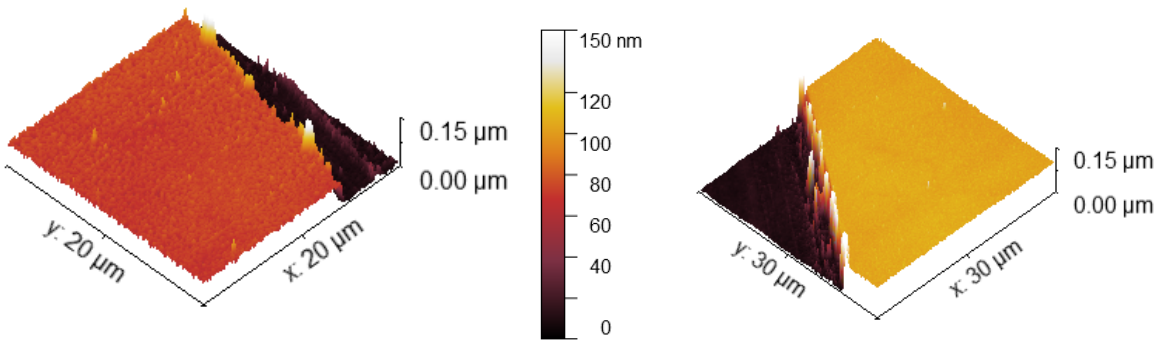

Figure 9: AFM micrographs of the devices with the pentacene and the C_{60} layers on top.

Figure 9 shows a $20\mu m \times 20\mu m$ section of the device with pentacene on top and a $30\mu m \times 30\mu m$ section of the device with C_{60} on top. We can notice the scratch on both films. With this resolution, both layers seem flat: the AFM analysis program reveals a roughness of 6.88 nm R.M.S and 6.35 nm R.M.S. As predicted, the device with the additional C_{60} layer is higher than the other device. To get more quantitative results about the device thicknesses, we have to turn to the second part of our AFM analysis.

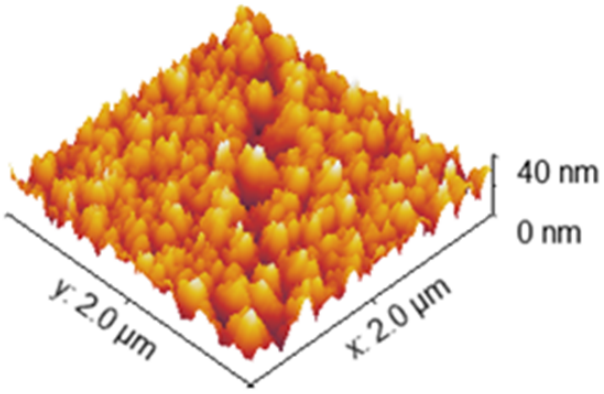

Figure 10: Highly resolved AFM micrograph of the device with pentacene as the top layer.

Before doing so, we want to look at the morphology of the pentacene layer in more detail, as it will set the basis for the most important interface in our overall device, the pentacene/C_{60} interface. We show in Figure 10 a $2\mu m \times 2\mu m$ section of the pentacene layer. At this higher level of resolution, we notice that upon evaporation, the pentacene film forms islands with diameters ranging from 50 nm to 200 nm. The AFM analysis program confirms a surface roughness of approximatively 7 nm R.M.S. In our EQE model, we suppose a planar heterojunction between pentacene and C_{60}, this is thus an approximation that we have to be aware of when using the model.

To determine the thickness of a layer, we scrap the films with a sharp needle and then use a histogram of heights to determine the step height between the scratched part and the films. Here, we can see from Figure 11 that the added contributions of PEDOT:PSS, P3HT and pentacene result in a global thickness of 64.1 nm, as measured by the difference between the peak at 73.1 nm and the scratch peak at 9 nm. Using the same method, we determine from Figure 12 that the added contributions of PEDOT:PSS, P3HT, pentacene and C_{60} result in a global thickness of 91.8 nm. From this, we can conclude that the thickness of the C_{60} layer -as measured by the difference between the 2 devices- is $\simeq 27.7$ nm. Within the experimental error bar, this is in good agreement with the expected thickness of 25 nm.

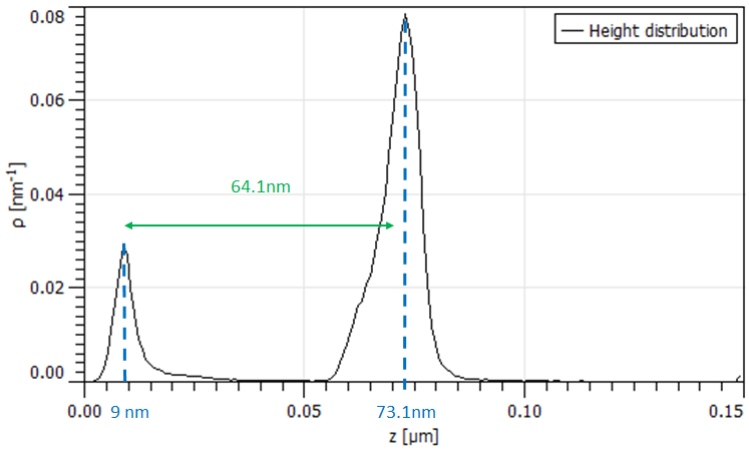

Figure 11: AFM measured histogram of heights of the device containing PEDOT:PSS, P3HT and pentacene.

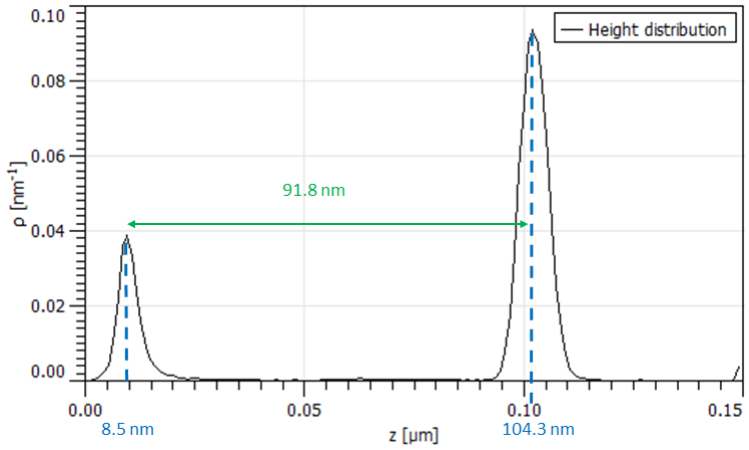

Figure 12: AFM measured histogram of heights of the device containing PEDOT:PSS, P3HT, pentacene and C_{60}.

4.2 Performance of the device

4.2.1 Current-voltage

Current-voltage characteristics gives four important parameters which serve to characterise an organic solar cell: the open-circuit voltage V_{OC}, the short-circuit current density J_{SC}, the power conversion efficiency η and the fill factor FF. To understand how these parameters characterize a solar cell, let us first describe the physical process behind each of these.

We start with the open-circuit voltage. The V_{OC} is the voltage associated with zero current flow. The total current measured is composed by three contributions, first the photocurrent (in direction towards the eletrodes), second the parasitic leakage current (with direction from the electrodes), and third any loss current due to geminate and non-geminate recombination of electrons and holes (with direction from the electrodes)[23]. In that case, V_{OC} indicates the voltage at which the photocurrent compensates leakage and recombination current, so that the total current measured under illumination is zero.

We now look at the short-circuit current density, which is the current measured when the voltage across the solar cell is 0. Under short-circuit conditions the work functions of the two electrodes equilibrate and an internal electric field builds up. Assisted by the internal field, the successfully separated charges drift to the corresponding electrode and can be extracted. These charges cause the photocurrent at zero voltage.

Electrical power is given by the product of current and voltage. The power density delivered from a solar cell per unit device area is $P_{out} = j(V) \times V$. A good measure for efficiency is the power conversion efficiency η. It is given by the ratio of the maximum electrical power delivered by the photocell per unit device area to the incident light power per unit device area: $\eta = \frac{P_{out,max}}{I(\lambda)}$.

The power delivered by the solar cell will be zero at short-circuit because the voltage is zero, and it will also be zero at open-circuit since there is no photocurrent. It will thus take a maximum value in between. This is the so-called maximum power point, where the rectangle defined by j(V)×V under the current-voltage curve has the largest possible area. This allows for the definition of a geometrical factor, the fill factor FF: $FF = \frac{J_{max} \times V_{max}}{J_{SC} \times V_{OC}}$. In a perfect solar cell, the fill factor will be as high as possible. Low fill factors are due to parasitic losses such as shunt and series resistances and are also caused by the fact that in organic photocells at low internal field, geminate and non-geminate recombination compete with charge extraction.

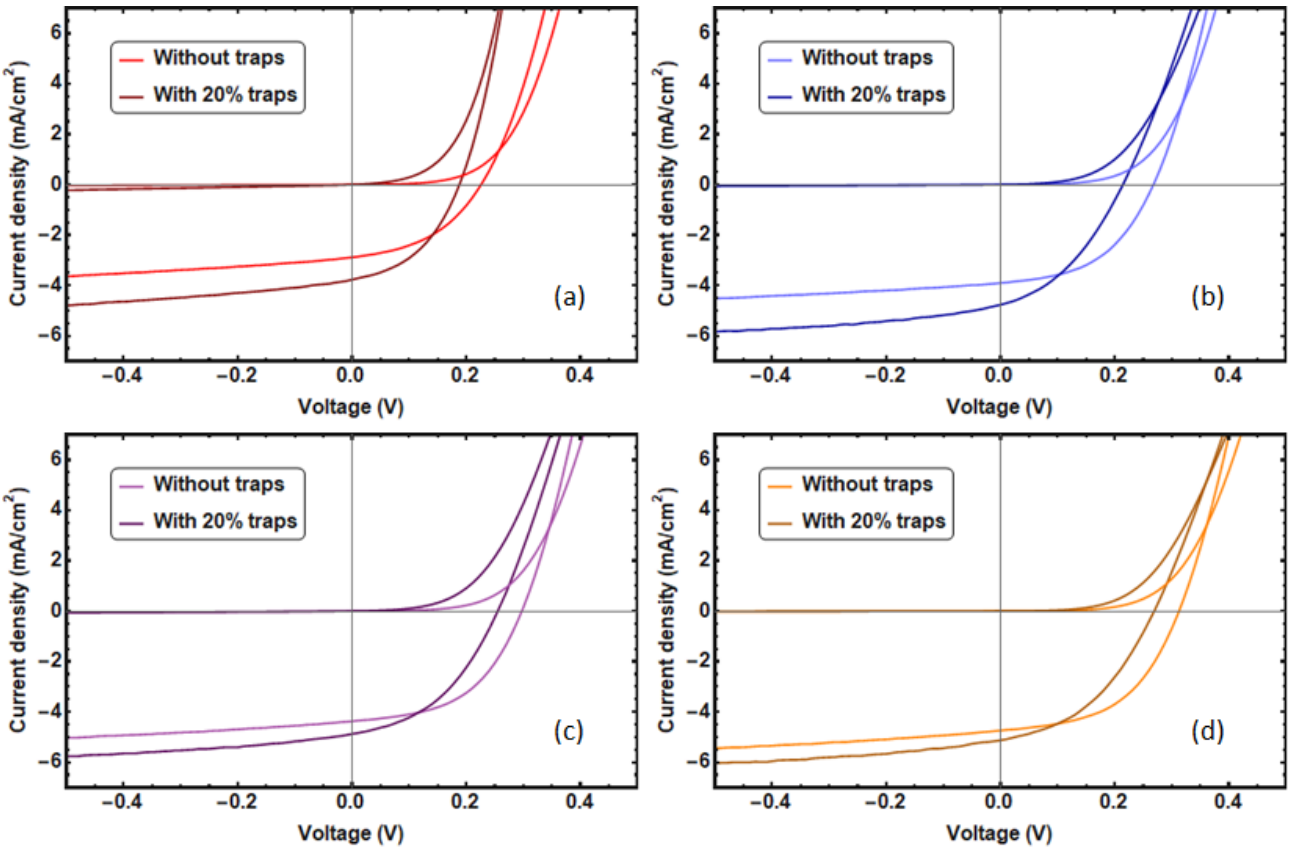

Figure 13: Dark and Light JV characteristics of devices containing a pure pentacene layer or a pentacene layer doped with 20% of pentacenequinone, for different layer thicknesses: (a) 20 nm, (b) 40 nm, (c) 60 nm and (d) 80 nm.

The dark and light JV characteristics of the best pixels in the devices made with a varying thickness of either a pure pentacene layer or a pentacene layer doped with 20% pentacenequinone are shown in Figure 13. The detailed trend for each important feature is presented in Figure 14.

The V_{OC} of the devices containing pentacenequinone are lower than those with pure pentacene: looking at Figure 14 (a), the median value for V_{OC} decreases from 0.23 to 0.19 V for the 20 nm thick layer, from 0.27 V to 0.21 V for the 40 nm thick layer, from 0.30 V to 0.26 V for the 60 nm thick layer and from 0.31 V to 0.27 V for the 80 nm thick layer. With added traps in the material, we expect higher recombination in the coevaporated devices, as the pentacenequinone molecules might act as a non-geminate recombination site within the material. As mentioned previously, V_{OC} represents the voltage at which the photocurrent compensates the leakage current and the recombination current. The trend for V_{OC} is consistent with this hypothesis: as traps are added in the device, the recombination current increases, thus decreasing the measured V_{OC} of the device, as seen in Figure 14 (a).

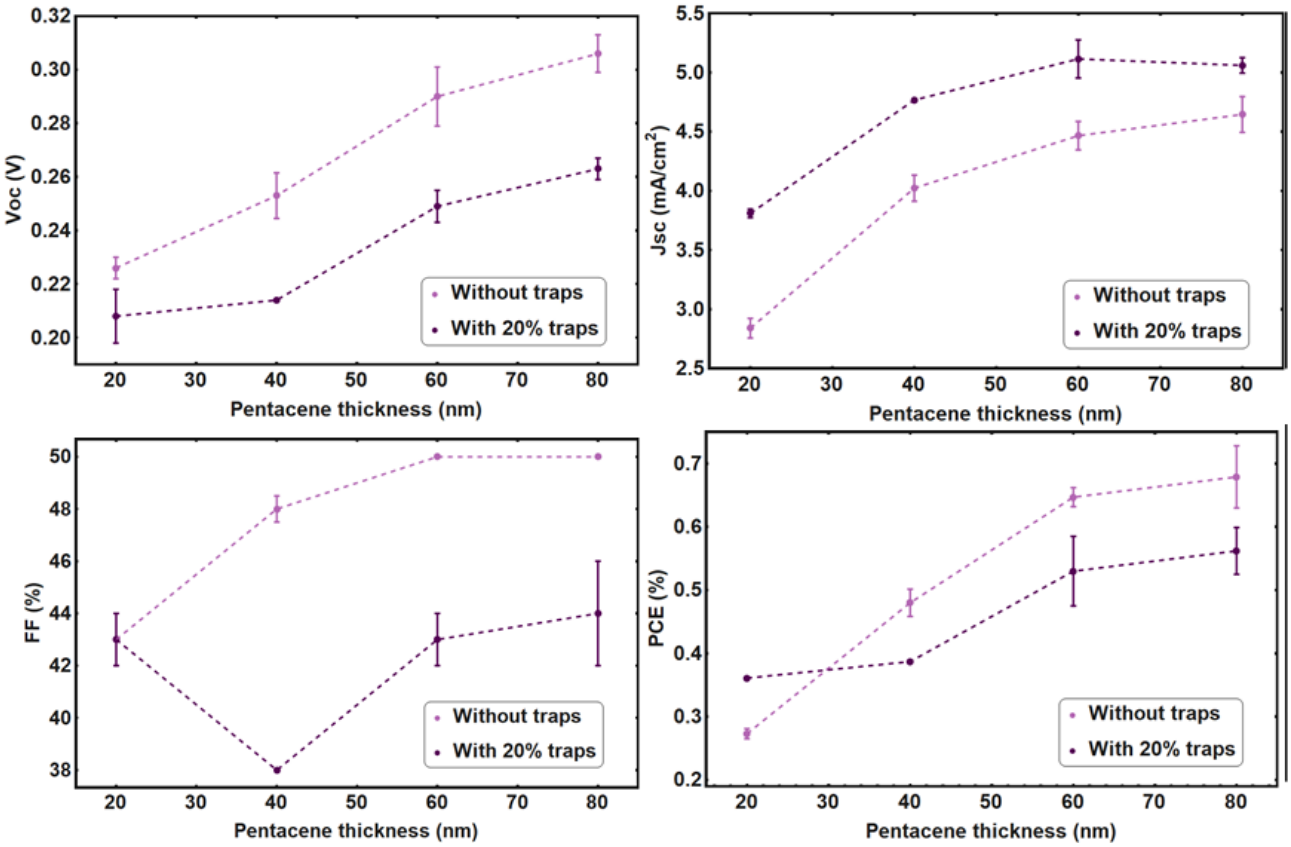

Figure 14: Detail of the trends found by JV characterisation: V_{OC}, J_{SC}, FF and PCE measured for either a pure pentacene layer or a pentacene layer doped with 20% of pentacenequinone, as a function of the thickness of the layer within the device. We measure multiple pixels and represent the median value by a dot and the median deviation by an error bar. The device with a 40 nm thick layer of pentacene coevaporated with traps is an exception as only one of the pixels out of the two solar cells made under these conditions worked. All other cases are presented with an error bar.

The J_{SC} of the devices containing pentacenequinone are higher than those with pure pentacene: looking at Figure 14 (b), the median value for J_{SC} increases from 2.87 mA/cm^2 to 3.78 mA/cm^2 for the 20 nm thick layer, from 3.91 mA/cm^2 to 4.77 mA/cm^2 for the 40 nm thick layer, from 4.88 mA/cm^2 to 4.37 mA/cm^2 for the 60 nm thick layer and from 4.74 mA/cm^2 to 5.13 mA/cm^2 for the 80 nm thick layer. With added traps in the material, our expectation was to see a decrease in J_{SC}, as less current is expected to flow between the electrodes. The trend shown in Figure 13 is thus contrary to what we expect. Different hypotheses may serve to explain this inconsistency. The pentacene layer degrades very rapidly, even under nitrogen atmosphere. During the coevaporation of pentacene with pentacenequinone, we leave the devices with spin coated pentacene in the glove box for about 2 hours, which may lead to an overall loss in this series of devices. Alternatively, as it is the first time we use pentacenequinone in the thermal evaporator, there might be some discrepancy between the tooling factors of pentacene and pentacenequinone, and our supposition that we have layers of

exactly the same thickness may in fact not hold true. In this case, the increase of J_{SC} would be a consequence of the increased thickness of the coevaporated layer, as the absorption of light in the layer is enhanced. Another hypothesis is that pentacenequinone might also be part of the series of organic semiconductors which exhibit singlet fission processes. Further investigation is needed to distinguish between these different hypotheses.

The second trend noticeable in Figure 14 (b) is the enhancement of J_{SC} with increasing pentacene thickness. The efficiency of the pentacene layer depends both on the generation of excitons and their decay. If the material is too thin, there will be insufficient absorption, but if the layer is too thick, the decay mechanisms within the layer will degrade the overall performance. Here, enhancement of J_{SC} with increasing pentacene thickness serves to prove we are in the former case, where the limiting factor is the absorption of the pentacene layer.

Looking at Figure 14 (c), we notice that the fill factor of the devices with added impurities is lower than that of the devices with pure pentacene. At low internal fields, recombination is the main cause in the loss of fill factor. Together with the V_{OC} trend, this is second evidence that traps lead to a higher recombination rate in the pentacene layer.

Looking at Figure 14 (d), we notice that the power conversion efficiency of the devices increases with increasing pentacene thickness. This is the combined consequence of an increase in V_{OC}, J_{SC} and FF for thicker pentacene layers. The power conversion efficiency of the devices with pure pentacene are overall higher than those of the devices with added impurities: this shows that in our specific case, the higher J_{SC} in the devices with 20% pentacenequinone do not compensate for the lower V_{OC} and lower FF. The difference in power conversion efficiency seems to increase with the thickness of the pentacene layer in the device, which is a possible indication for a difference in the diffusion length.

4.2.2 External quantum efficiency

The EQE is an important measurement for a solar cell, as it provides information about its electronic and optical properties. Specifically, the EQE helps in recognising the areas in the solar spectrum which are suffering from loss mechanisms, either from a light management perspective or from a carrier management perspective. Combining pentacene and C_{60}, Congreve *et al*[24] published the first demonstration of a solar cell with EQE over 100%, unambiguously demonstrating singlet exciton fission. The IQE serves to complete EQE characterisation as it decouples the electronic properties

from the optical properties. However our focus in this part remains the EQE, because we use it as an indirect measurement for the diffusion length of triplet excitons.

We show in Figure 15 the EQE curves of devices of varying thickness containing a pure pentacene layer or a pentacene layer doped with 20% of pentacenequinone. Correlated with the increase of J_{SC} seen in the JV characteristics, we observe an enhancement of the EQE when adding 20% traps to the composition of the pentacene layer. This effect is more pronounced for the thiner devices than for the thicker ones, reaching almost identic curves for the 80 nm thick device. With the JV characteristics, this is the second evidence for a higher current flowing through the devices with additional impurities. As mentioned in the previous section, this result is surprising, specifically considering an amount as high as 20% of traps, and calls for further investigation.

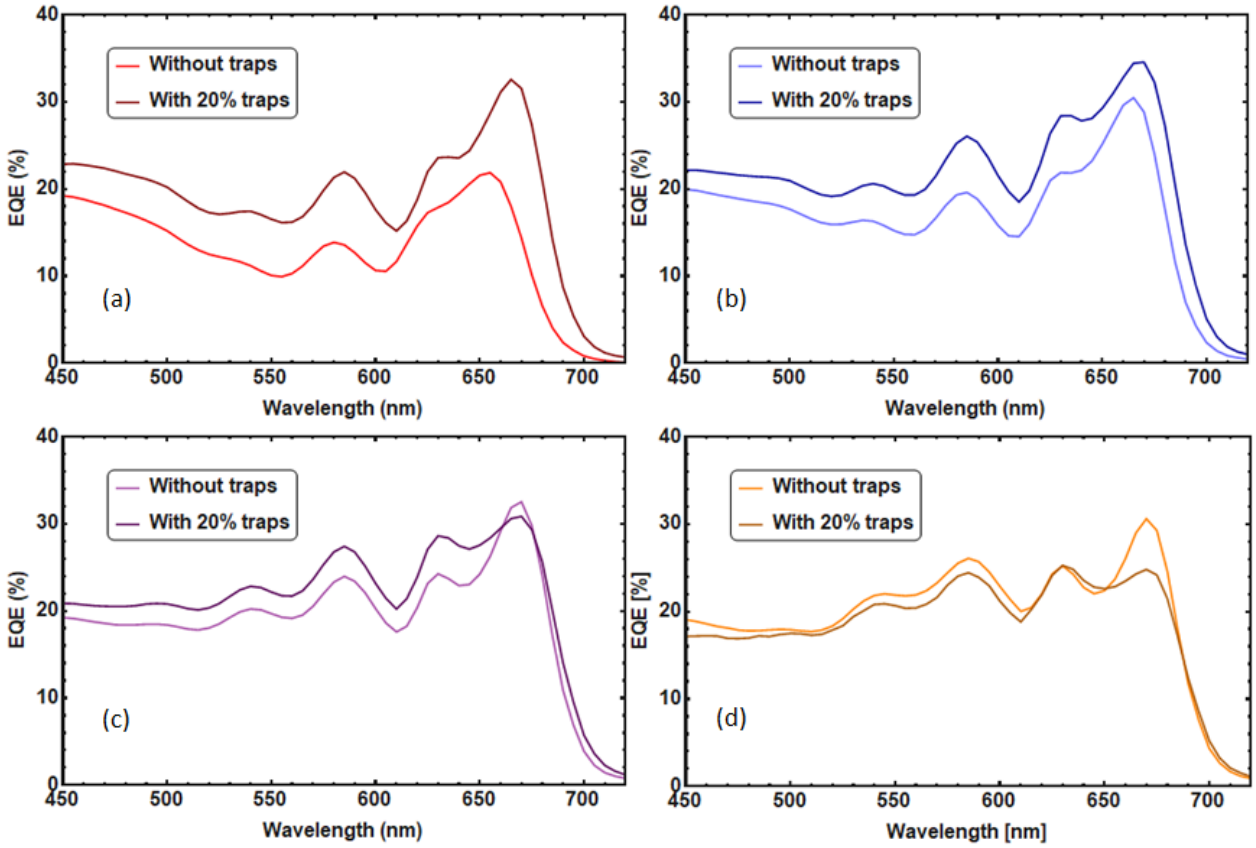

Figure 15: EQE curves of devices containing a pure pentacene layer or a pentacene layer doped with 20% of pentacenequinone, for different layer thicknesses : (a) 20 nm, (b) 40 nm, (c) 60 nm and (d) 80 nm.

4.3 Optimisation of parameters of the model

As mentioned in the methods section, there are 4 fitting parameters in the model we develop to calculate EQE: the two efficiencies η_{pent} and $\eta_{C_{60}}$ for the dissociation of excitons formed in the pentacene layer and in the C_{60} layer, the efficiency η_{P3HT} for the injection of excitons from P3HT to pentacene and the exciton diffusion length L_{pent} of the triplet excitons in pentacene.

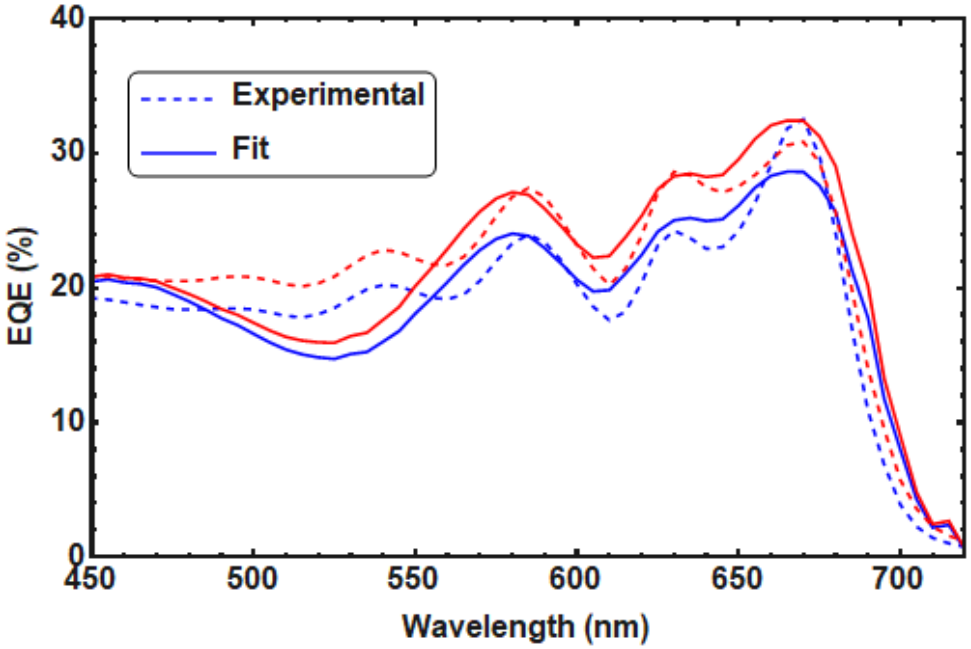

Figure 16: Comparison of modeled with experimental EQE curves for the 60 nm thick layer of pure pentacene (blue curve) and pentacene doped with 20% of pentacenequinone (red curve). The diffusion length L_{pent} used in the model is 15 nm for both modeled curves, the P3HT injection efficiency η_{P3HT} used is 30%, the C_{60} dissociation efficiency used is 32% and the pentacene dissociation efficiency $\eta_{C_{60}}$ is fixed at 60% for the pure pentacene modelled curve and at 68% for the coevaporated pentacene modelled curve.

The model shows relative agreement with the experimental data when using a diffusion length of $L_{\text{pent}} = 15$ nm, as can be seen from Figure 16, which shows the calculated and experimental EQE curves for the devices containing the 60 nm-thick pentacene layer with and without traps. Indeed, the three important peaks, located at $\lambda = 585$ nm, $\lambda = 635$ nm and $\lambda = 660$ nm, and their expected height (exception made of the peak at $\lambda = 660$ nm) are retrieved for both the EQE curves of the device with pure pentacene and the device with impurities. We loose however the small peak located at $\lambda = 545$ nm and globally the area of the spectrum between $\lambda = 460$ nm and $\lambda = 580$ nm.

Overall, we need to point out the severe limitations we experience when using our model to estimate accurately the triplet exciton diffusion length. We estimate the quality of the fit using

$$\int_{\lambda_{min}}^{\lambda_{max}} \frac{1}{\lambda_{max}-\lambda_{min}} \times \frac{EQE_{mod}(\lambda)-EQE_{exp}(\lambda)}{EQE_{exp}(\lambda)}$$

For each experimental curve, we calculate about 500 different combinations by varying η_{P3HT}, η_{pent} and L_{pent}. $\eta_{\mathrm{C_{60}}}$ can be fitted separately. Specifically, η_{P3HT} is varied between 14% and 76% with a 4% resolution, η_{P3HT} is varied between 14% and 76% with a 2% resolution and L_{pent} is varied between 10 nm and 35 nm with a 1 nm resolution. In the second part of the calculation, $\eta_{\mathrm{C_{60}}}$ is varied between 10% and 40% with a 4% resolution. We compare the experimental curve and calculated curve for each calculated EQE curve and for each cell. The aim is to find a global fit with a set of fixed parameters that is consistent with all cells within the pure pentacene series, and a different set of fixed parameters consistent with all cells within the pentacene with added impurities series.

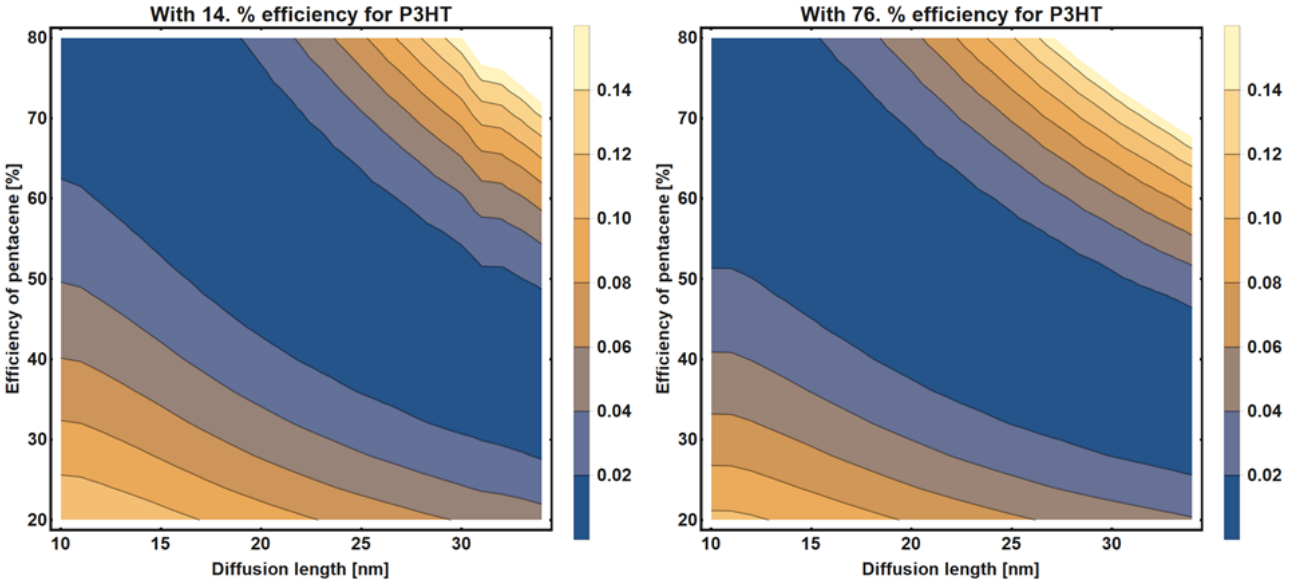

Figure 17: 2D graphs representing the quality of the fit as a function of η_{pent} and L_{pent}, for the device with a 80 nm thickness of pure pentacene, and considering two values for η_{P3HT} of 14% and 76%.

Figure 17 shows two 2D graphs representing the quality of the fit as a function of η_{pent} and L_{pent}, for the device with a 80 nm thickness of pure pentacene. To represent the quality of the fit as a function of η_{P3HT}, we show two of these 2D graphs, each representing one of the extreme values of η_{P3HT}, i.e. 14% and 76%. The first observation is that both 2D graphs look very much alike, and thus do not allow a precise estimation of η_{P3HT}. The second observation is that the quality of the fit seems good in two different cases: either if η_{pent} is high and L_{pent} is low, or if η_{pent} is low and L_{pent} is high. The trend is similar for the devices with pentacene thicknesses of 20 nm, 40 nm and 80 nm.

This means that for our series of devices, our model does not allow us to discriminate between a high efficiency of pentacene dissociation at the interface and a short diffusion length of the triplet excitons within the pentacene layer. The implication is that even if our model can reproduce the experimental curves to some extent, we cannot use it here as an effective way of measuring the diffusion length of triplet excitons. We can think of three different reasons why this might be the case. First, the crystal formation within the layer might change for different thicknesses of pentacene, thereby changing the distance and orientation between two neighbouring molecules. Second, our use of the standard n and k values for the materials might not be justified in our case. Finally, it is also possible that the scattering of light on the pentacene matrice and on the pentacene-pentacenequinone matrice is different. We try to see if our model can still give us some minimal information considering a factor C defined by $\mathrm{C} = L_{\mathrm{pent}} \times \eta_{\mathrm{pent}}$.

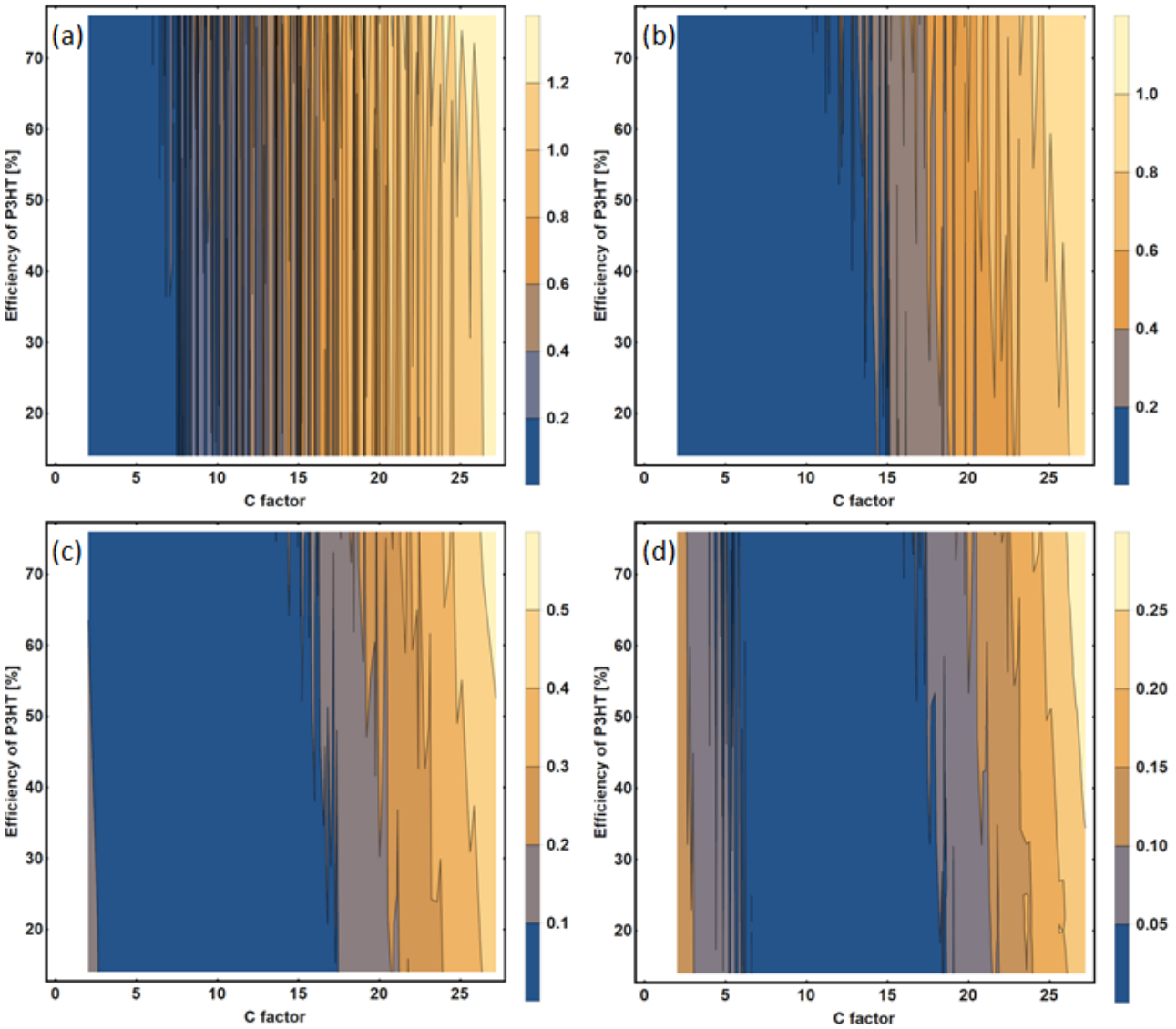

Figure 18: 2D graphs representing the quality of the fit as a function of $\mathrm{C} = L_{\mathrm{pent}} \times \eta_{\mathrm{pent}}$ and η_{P3HT}, for devices with a pure pentacene layer of thickness (a) 20 nm, (b) 40 nm, (c) 60 nm and (d) 80 nm.

We represent in Figure 18 four 2D graphs, representing the quality of the fit with the EQE experimental curves as a function of C and η_{P3HT}. The four graphs represent the devices with pentacene layer of thickness (a) 20 nm, (b) 40 nm, (c) 60 nm and (d) 80 nm. The first observation is than in all four graphs, η_{P3HT} has a very limited impact on the quality of the fit, simply allowing for slightly larger C factors at low η_{P3HT}. The second observation is that there is a trend of increasing C factor when moving from the thinner devices to the thicker devices.

5 Conclusion

Acknowledgements

I would like to thank Bruno Ehrler for the great quality of his scientific supervision. I am grateful to Moritz Futscher for teaching me every possible aspect of the experiments and following the daily aspects of my project. I also want to thank Jumin Lee who helped me a lot with his knowledge of the experimental setups. Finally, I wish to thank to whole Hybrid Solar Cells group for the interesting discussions and providing for a happy place of work. I am happy to be back soon!

References

[1] B. O'Regan and M. Gratzel, *Nature*, **1991**, *353*, 737-740, **A low-cost, high-efficiency solar cell based on dye-sensitized colloidal TiO_2 films**.

[2] W. Chan, T.C. Berkelbach, M.R. Provorse, N.R. Monahan, J.R. Tritsch, M. Hybertsen, D.R. Reichman, J. Gao, and X.Y. Zhu, *Acc. Chem. Res.*, **2013**, *46*, 1321, **The Quantum Coherent Mechanism for Singlet Fission: Experiment and Theory**.

[3] W.L. Chan, M. Ligges, A. Jailaubekov, L. Kaake, L. Miaja-Avila and X.Y. Zhu, *Science*, **2011**, *334*, 1541, **Observing the Multiexciton State in Singlet Fission and Ensuing Ultrafast Multi-Electron Transfer**.

[4] A.A. Bakulin, S.E. Morgan, T.B. Kehoe, M.W. B. Wilson, A.W. Chin, D. Zigmantas, D. Egorova and A. Rao,*Nat. Chem.*, **2015**, *8*, 16, **Real-time observation of multiexcitonic states in ultrafast singlet fission using coherent 2D electronic spectroscopy**.

[5] J. Xia, S.N. Sanders, W. Cheng, J.Z. Low, J. Liu, L.M. Campos and T. Sun, *Adv. Mater.*, **2017**, 16016528, **Singlet fission: Progress and Prospects in Solar Cells**.

[6] M. Tabachnyk, B. Ehrler, S. Gélinas, M.L. Bohm, B.J. Walker, K.P. Musselman, N.C. Greenham, R.H. Friend and A. Rao, *Nature Materials*, **2014**, *13*, 1033-1038, **Resonant energy transfer of triplet excitons from pentacene to PbSe nanocrystals**.

[7] Website of our group, *https://amolf.nl/research-groups/hybrid-solar-cells/research-activities*.

[8] W. Shockley and H.J. Queisser, *Journal of Applied Physics*, **1961**, *32*, 510-519, **Detailed balanced limit of efficiency of p-n junction solar cells**.

[9] M.B. Smith and J. Michl, *Chemical Reviews*, **2010**, *110*, 6891-6936, **Singlet Fission**.

[10] M.W.B. Wilson, A. Rao, J. Clark, R.S. Santosh Kumar, D. Brida, G. Cerullo and R.H. Friend, *J. Am. Chem. Soc.*, **2011**, *133*, 141830-11833, **Ultrafast Dynamics of Exciton Fission in Polycrystalline Pentacene**.

[11] N. Koch, I. Slazmann, R.L. Johnson, J. Pflaum, R. Fiendlein qnd J.P. Rabe, *Org. Elec.*, **2006**, *7*, 537-545, **Molecular orientation dependent energy levels at interfaces with pentacene and pentacenequinone**.

[12] O.D. Jurchesku, J. Baas and T.T.M. Palstra, *Appl. Phys. Lett.*, **2004**, *84*, 30613, **Effect of impurities on the mobility of single crystal pentacene**.

[13] M. Tabachnyk, B. Erhler, S. Bayliss, R.H. Friend and N.C. Greenham, *Applied Physics Letters*, **2013**, *103*, 153302, **Triplet diffusion in singlet exciton fission sensitized pentacene solar cells**.

[14] B. Ehrler, B.J. Wlaker, M.L. Boehm, M.W.B. Wilson, Y. Vaynzof, R.H. Friend and N.C. Greenham, *Nat. Comm.*, **2012**, *3*, 10193, **In situ measurement of exciton energy in hybrid singlet-fission solar cells**.

[15] B. Ehrler, M.W.B. Wilson, A. Rao, R.H. Friend and N.C. Greenham *Nano Lett.*, **2012**, *12*, 1053-1057, **Singlet Exciton Fission-Sensitized Infrared Quantum Dot Solar Cells**.

[16] S. Yoo, B. Domercq and B. Kippelen, *Appl. Phys. Lett.*, **2004**, *85*, 5427, **Efficient thin-film organic solar cells based on pentacene/C_{60} heterojunctions**.

[17] G.F. Burkhard, E.T. Hoke and M.D. McGehee, *Adv. Physics Mater.*, **2010**, *22*, 3293–3297, **Accounting for Interference, Scattering, and Electrode Absorption to Make Accurate Internal Quantum Efficiency Measurements in Organic and Other Thin Solar Cells**.

[18] M. Tabachnyk, *Research Project Master Thesis*, **Triplet Exciton Dynamics in Pentacene**.

[19] D. L. Dexter, *J. Chem. Phys.*, **1951**, *21*, 836–850, **A Theory of Sensitized Luminescence in Solids** .

[20] O. V. Mikhnenko, P.W.M. Blom and T-Q. Nguyen, *Energy Environ. Sci.*, **2015**, *8*, 1867, **Exciton diffusion in organic semiconductors**.

[21] H. Wang, H-Y. Wang, B-R. Gao, L. Wang, Z-Y. Yang, X-B. Du, Q-D. Chen, J-F. Song and H-B. Sun, *Nanoscale*, **2011**, *3*, 2280-2285, **Exciton diffusion and charge transfer dynamics in nano phase-separated P3HT/PCBM blend films**.

[22] P. Peumans, A. Yakimov and S.R. Forrest, *J. Appl. Phys.*, **2003**, *93*, 3693, **Small molecular weight organic thin-film photodetectors and solar cells**.

[23] A. Kohler and H. Bassler, *Wiley-Wch*, **2015**, **Electronic Processes in Organic Semiconductors**.

[24] D.N. Congreve, J. LEE, N.J. Thompson, E. Hontz, S.R. Yost, P.D. Reusswig, M.E. Bahlke, S. Reineke, T.V. Voorhis and M.A. Baldo, *Science*, **2013**, *340*, 334-337, **External Quantum Efficiency Above** 100% **in Singlet-Exciton-Fission-Based Organic Photovoltaic Cell**.